Int J Adv Manuf Technol (2014) 75:1605–1612
DOI 10.1007/s00170-014-6242-4

ORIGINAL ARTICLE

Numerical simulation and experiment study on hollow spinning process for square cross-section cone

Z. Jia · Z. R. Han · Q. Xu · W. F. Peng

Received: 30 March 2014 / Accepted: 4 August 2014 / Published online: 26 August 2014

Abstract Spinning process is investigated to reveal the mechanism of square cross-section spinning without mandrel. The finite element model with the roller path formula as a boundary condition is established. Forge3D software is used to simulate the spinning process, and the accuracy of the finite element model is verified through experiment. From the stress–strain field, the residual stress on the surface of the workpiece is small after square cross-section cone hollow spinning and the maximum deformation locates on the middle part of the slope surfaces of the workpiece. The strain field distribution and the same Δr in different rotation round are the cause of the slight curvature that appears on the cross-section edge. The wall thickness decreases after hollow spinning, and the upper wall thickness is larger than the lower part.

Keywords Hollow spinning · Square cross-section cone · Roller path · Numerical simulation

1 Introduction

Spinning process is an ancient metal forming technology used to manufacture hollow products from metal sheets or tubes [1–6]. In recent years, Kwiatkowski et al. [2] derived two roller path design principles for die-less necking-in tubes spinning based on the theoretical analysis and pointed out that the wall thickness distribution of such products is influenced primarily by the roller path. In oblique shear spinning process, Akio and Hirohiko [5] tried to control the wall thickness distribution and claimed that the synchronous die-less spinning method is suitable for varying the wall thickness. Wang and Long [7, 8] studied conventional multi-pass shear spinning process and pointed out that the wall thickness of the workpiece decreases gradually after each forward roller pass. The investigations above show that the hollow spinning is flexible for many products, and it is an important topic to discuss that the wall thickness distribution is impacted deeply by roller path.

With the development of spinning processing, some complex multi-pass rotational products were manufactured by spinning [9–12]. For example, Lin et al. [9] developed multi-pass draw-spinning process of hyper-hemispherical shell through experiment. Thin-walled tubular parts with longitudinal inner ribs formed by spinning were proposed by Jiang et al. [10, 11]. In the last few years, non-axisymmetrical tubes processed by spinning were developed by Xia et al. [12–14]. All of these researches demonstrate that roller path plays a decisive role for the parts with complex geometric features. On the other hand, some researches were carried out on non-circular cross-section spinning. For example, Lai and Xia et al. [15] investigated the spinning process of the hollow cone with triangular cross-section and revealed its stress and strain distributions. Wu [16] simulated the hollow part with four arc-typed cross-section spinning process and compared it with the triangular cross-section one. Shimizu [17] derived the roller path for elliptical cone formed by synchronous spinning.

The square cross-section cone is one of non-circular cross-section hollow parts as shown in Fig. 1 and might be applied in aviation, aerospace, and automotive industries. The forming mechanism and process of non-circular cross-section hollow parts spinning were revealed, and the force in the deforming process was also analyzed in previous investigations [18]. But

Z. Jia · Z. R. Han (✉) · Q. Xu
Key Lab of Fundamental Science for National Defense of Aeronautical Digital Manufacturing Process, Shenyang Aerospace University, Shenyang 110136, Peoples' Republic of China
e-mail: hanren888@163.com

Z. Jia
e-mail: zjia@alum.imr.ac.cn

W. F. Peng
Zhejiang Provincial Key Lab of Part Rolling Technology, Ningbo University, Ningbo, Zhejiang, China

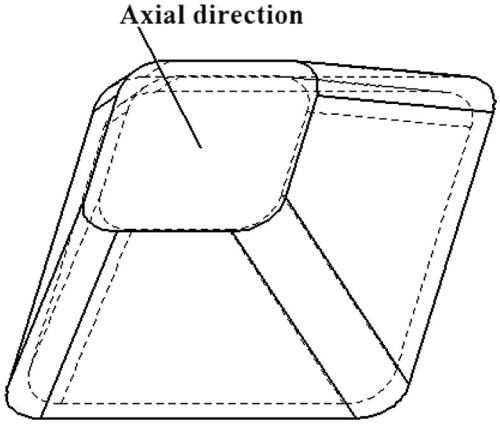

Fig. 1 Sketch of square cross-section cone

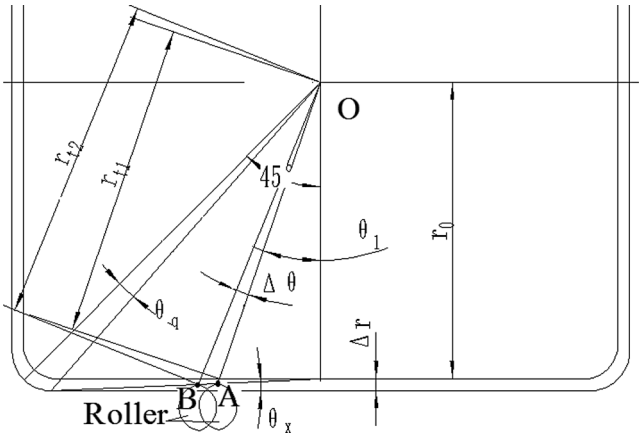

Fig. 2 Roller position in the one-path spinning process

there are still some problems to be solved for the square cross-section cone: firstly, the cross-section edge of the part investigated previously was not straight (it was arcs); secondly, the anterior non-circular spinning needed a mandrel die and this led to the high cost and long production cycle of the spinning process. If a corresponding-shape mandrel die is used, it must be modified according to the amendment of the geometric parameters of the square section cone, which leads that the preparation cycle is extended and the cost of manufacturing process increases. Therefore, a hollow spinning method for the square cross-section cone forming is investigated in this paper.

2 Roller path

Because of the geometry characteristics of square cross-section, the roller needs radial direction feed while the axial feed is running and there is a precise mathematical relationship between the roller path and the spindle speed forming the square shape. Figure 2 shows the roller position in one-pass spinning process. Through a tiny period $_{\Delta t}$, the roller moves a short distance $_{\Delta L}$ along the radial direction. Corresponding to the square cross-section, the roller movement is from point A to point B. With the rollers moving, the spindle rotates a small angle $_{\Delta\theta}$ and at the same time the roller goes for a minute distance along the axial direction. ΔL is given by

$$\Delta L = r_{t1} - r_{t2} \tag{1}$$

$$\Delta t = \frac{\Delta L}{v_x} = \frac{\Delta\theta}{360} \times \frac{1}{s} \tag{2}$$

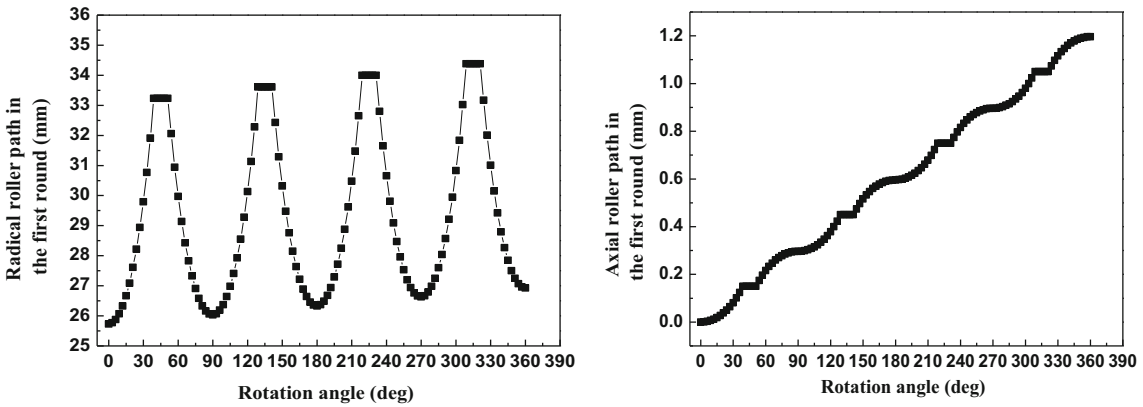

(a) Radical roller path (b) Axial roller path

Fig 3 Roller path in the first rotation round. **a**, **b**

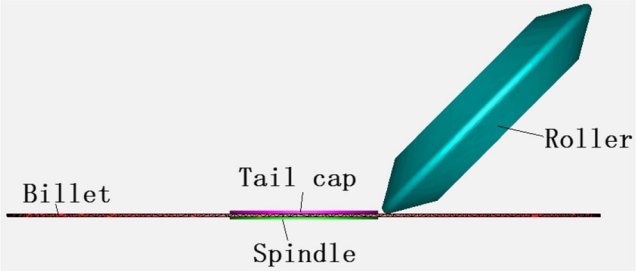

Fig. 4 3D geometric model of square cross-section cone spinning

where v_x is axial velocity of the roller, s is the rotation speed of the spindle; r_{t1} is the distance between the roller contacting point with the workpiece and the rotation center O at the moment t_1 (the length of $\overline{OA}$); r_{t2} is the distance between the roller contacting point with the workpiece and the rotation center O at the moment t_2 (the length of $\overline{OB}$). θ_x is expressed as

$$\theta_x \arctan\left(\frac{\Delta r}{(r_0 \Delta r)\cot(45-\theta_q)}\right) \tag{3}$$

where θ_x is a reference angle shown in Fig. 2, Δr is the radical distance moved by the roller when the spindle rotates 45°; r_0 is half length of the initial square border; θ_q is the interim angle of the square cross-section.

Then r_{t1} and r_{t2} are, respectively expressed as

$$r_{t1} = \frac{r_0 \cos\theta_x}{\cos(\theta_x + \theta_1)} \tag{4}$$

$$r_{t2} = \frac{r_0 \cos\theta_x}{\cos(\theta_x + \theta_1 + \Delta\theta)} \tag{5}$$

Further, Δr and $\Delta\theta$ are equivalent to step size per revolution and the smaller value they are set the closer to a straight line the relative path is. Meanwhile, the ratio of Δr and Δz (axial feed of the roller per rotation angle) determines the taper of the cone. Other parameters such as θ_q and r_0 are determined by the shape of the part.

Table 1 Geometric parameters of the billet, spindle, and tail cap

Parameters	Billet	Spindle	Tail cap	Roller
Diameter (mm)	280	50	50	100
Thickness (mm)	1	Null	Null	Null
Tip radius (mm)	Null	Null	Null	2

Table 2 Chemical components of Al99

Alloying addition	Si	Fe	Cu	Mn	Zn
Percentage (%)	0.225	0.25	0.125	0.025	0.05

By substituting Eq. (1), (3), (4), and (5) into Eq. (2), the relation between the rotation velocity of the spindle and the radical path of the roller in the first 45° of the spindle rotation is obtained. For the next 45°, the roller comes back on the radical direction and the formulas are used in a reverse direction. And in the following 45°, the roller goes away from the rotation center again, the formulas are almost the same but the initial square border becomes $2(r_0+2\Delta r)$. Thus, the following roller path in Fig. 3 will be gotten. Based on this principle, the roller path in unlimited rotation round can be deduced.

3 3D-FE model of hollow spinning process for square cross-section cone

3.1 3D geometric model

The 3D geometric model for the spinning process is composed of billet, spindle (not a mandrel), tail cap, and roller. They are assembled as a system of the spinning process of square cross-section cone in Forge3D software as shown in Fig. 4. The geometric parameters of the parts in the system are listed in Table 1. The angle between the rotation axis of the roller and the spindle is 45°.

3.2 Material constitutive model

The material of the billet is Al99 which is derived from the "Rheology Database" of Forge3D software, and its chemical

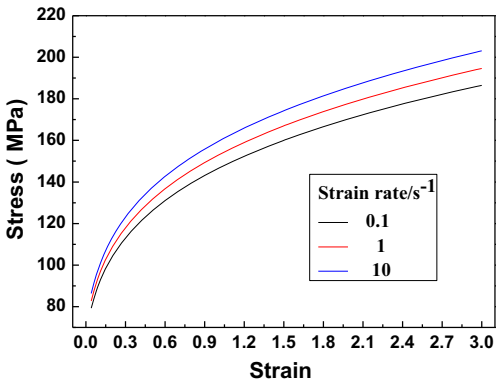

Fig. 5 Stress–strain curves of Al99 at 20 °C

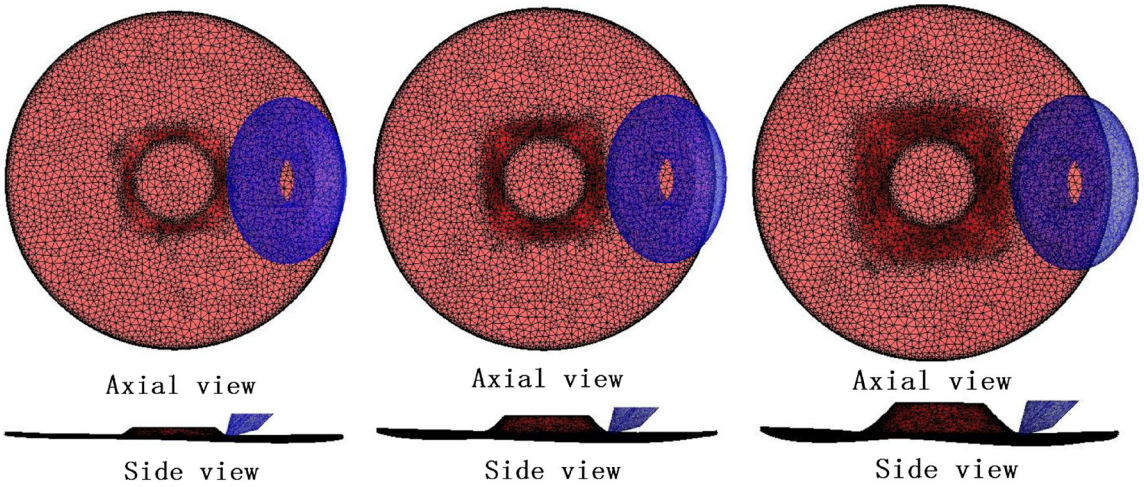

(a) Spinning time 9s (b) Spinning time 18s (c) Spinning time 30s

Fig. 6 Deformation process of the spinning. **a** Spinning time 9 s **b** Spinning time 18 s **c** Spinning time 30s

components are shown in Table 2. The constitutive model of Al99 corresponds with the following equation:

$$\sigma_f = Ae^{m_1 T} T^{m9} \varepsilon^{m_2} e^{m_4/\varepsilon} (1+\varepsilon)^{m_5 T} e^{m_7 \varepsilon} \varepsilon^{m3} \varepsilon^{m_8 T} \quad (6)$$

where T is the temperature, σ_f is the stress, ε is the strain, $\dot{\varepsilon}$ is the strain rate, A, m_1, m_2, m_3, m_4, m_5, m_7, m_8, and m_9 are the regression coefficients and A=161.96, m_1=−0.21×10^{-2}, m_2=0.22, m_3=0.019, m_4=0.44×10^{-2}, m_5=0, m_7=0, m_8=0, and

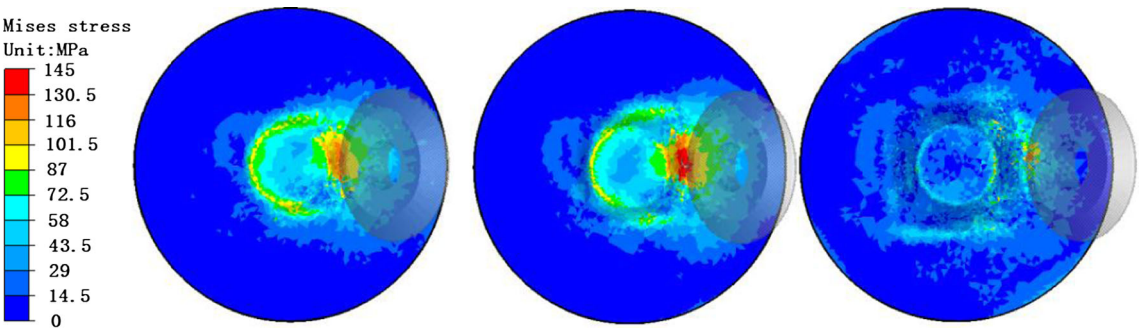

(a) Spinning time 9s (b) Spinning time 18s (c) Spinning time 30s

Fig. 7 Distribution of stress in the spinning process. **a** Spinning time 9 s **b** Spinning time 18 s **c** Spinning time 30 s

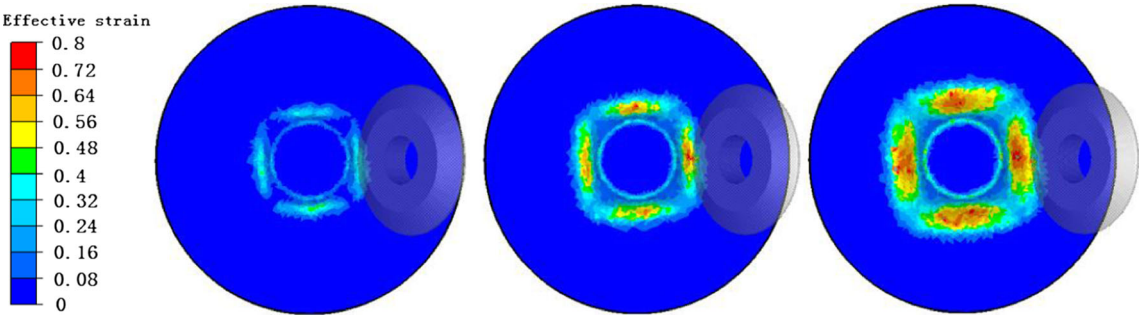

(a) Spinning time 9s (b) Spinning time 18s (c) Spinning time 30s

Fig. 8 Distribution of strain in the spinning process **a** Spinning time 9 s **b** Spinning time 18 s **c** Spinning time 30 s

Fig. 9 PS-CNCSXY 5-axis CNC spinning machine

$m9=0$. Figure 5 shows that the true stress–strain curves at the strain rate 0.1, 1, $10s^{-1}$, at 20 °C and the Young's modulus of the metal is 73 GPa and Poisson's ratio is 0.3.

3.3 Other boundary conditions

The temperature of the billet is 20 °C in the whole deforming process. The billet is refined with a tetrahedral mesh and the number of the meshes is 17,390. All the dies are set as rigid. The rotation velocity of the spindle is 30 r/min and with the velocity as the initial value, the roller path is imported into the software. A 6-t force is applied on the tail cap, and the friction coefficient between the billet and the tail cap is set to zero. The friction coefficient between the billet and the spindle is 0.4 implying no lubrication. The reason of such settings is that the billet can rotate with the spindle at the same speed without hindering from the tail cap. The lubricant between the workpiece and the roller is oil and the friction coefficient is 0.1. Then the finite element model is established.

4 Results and discussions

4.1 Deformation process by simulation

Figure 6 shows the deformation process of the square cross-section cone. It can be obviously seen that the cross-section forms a square gradually with the growing of the axial length of the workpiece. Furthermore, the edge of the square increases when the roller moves far away from the rotation center, meaning that the square shape of the cross-section becomes a little bigger as the workpiece rotates 360°. So, the deformation process illustrates that the roller path formula runs accurately.

4.2 Distribution of stress and strain

Figure 7 and Fig. 8 show the Mises stress and effective strain fields in spinning process. Large stress exists at the external surface of the contacting area between the roller and the workpiece and then the stress turns to a small value immediately as the material deviate from the contact zone. Under the blocking action of the tail cap and the dragging action of the roller, an arc shape stress area exists at the edge of the tail cap. When the spinning process is over, there is small residual stress leaving on the surface of the workpiece. After the spinning process starts, the deformation happens on the contacting zone firstly and then extends along the edge of the square cross-section. In the initial few seconds, a uniform distribution of strain filed exists on the straight edge but as the deforming process goes on, bigger deformation appears on the middle of the straight edge and at the last, the maximum deformation locates on the axisymmetric center area of the slope surfaces. Four slope surfaces have four maximum deformation areas. The reasons for the strain field distribution are that: (1) In order to form the straight edge, the roller must move forward and

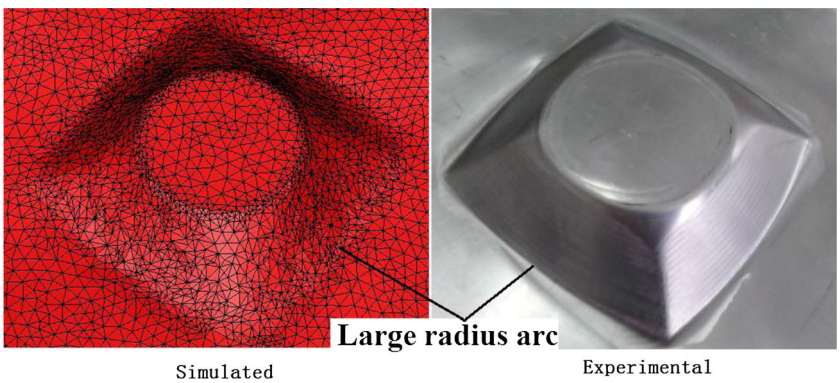

Fig. 10 Contrast of simulation and experimental results

backward on the radial direction. (2) In the first 1/4 of one spinning rotation round, the roller locates on one end of the straight edge which is the farthest position from the rotation center, and then the roller goes closer to the rotation center and pushes the material. (3) When the roller arrives at the middle of the straight edge where the nearest position from the rotation center is, the material of that position accumulates the biggest deformation. (4) In the period of the roller going to the other straight edge end, the metal which contacts the roller no longer suffers so big pressure and deforms slightly. According to the principle of volume invariably during deforming, larger effective strain means the material is flatter and longer, as a result, the wall thickness of the middle part on the slope plate of the "pyramid" cone reduces more seriously, on the other hand, the longer metal on the middle area makes the side of the cross-section become a large radius arc.

4.3 Comparison of the final shape

In order to verify the simulated result, the roller path used in simulation is written into CNC program for the spinning experiment. The experiment is carried out on PS-CNCSXY 5-axis CNC spinning machine (see Fig. 9). The shape comparison between the simulation and the experiment results is shown in Fig. 10.

Table 3 reveals the comparison of some key geometric dimensions between the experimental and the simulated results; Fig. 11 is the diagram of the key geometric dimensions. The result demonstrates a good agreement between the simulation and the experiment—both of them have a "pyramid without top" shape and maximum deviation of the key geometric dimensions is no more than 5 %. The shape comparison also confirms the accuracy of the finite element model. But the edge of the square cross-section is not very straight and presents a large radius arc. Apart from the strain field, the same Δr in different rotation round also caused the large radius arc phenomenon. Based on the same value of Δr, the roller path in the 90° of one rotation round cannot be a straight line but a broken line on the trapezoidal slope of the square section cone, and the intersection point of the two broken lines is on the middle of the roller path. Coupled with the action of the feeding space in the screws, the large radius arc phenomenon occurred.

Table 3 Comparison of the key geometric dimensions from simulation and experiment

Key geometric dimensions	Initial radius r_0/mm	Height of the cone (h/mm)	Direction	Final straight edge length (L/mm)
Experimental	26.6	16.1	0°	77.2
			90°	78.3
			180°	77.5
			270°	77.4
Simulated	25.8	16	0°	77.7
			90°	79
			180°	78.3
			270°	78.5

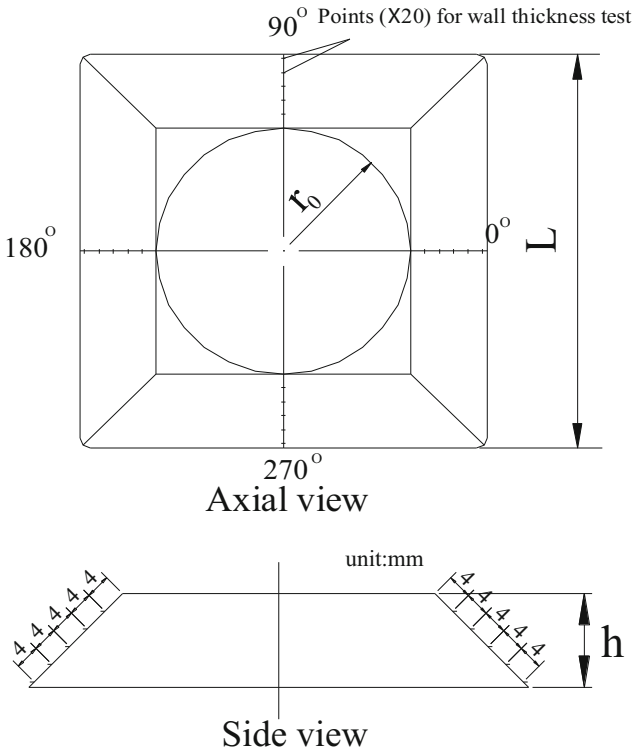

Fig. 11 Diagram of the key geometric dimensions

4.4 Wall thickness distribution

In order to inspect wall thickness distribution after spinning, the wall thickness is measured at 20 points and the positions of the points are illustrated in Fig. 11 (The workpiece is divided into four parts evenly and then the wall thickness

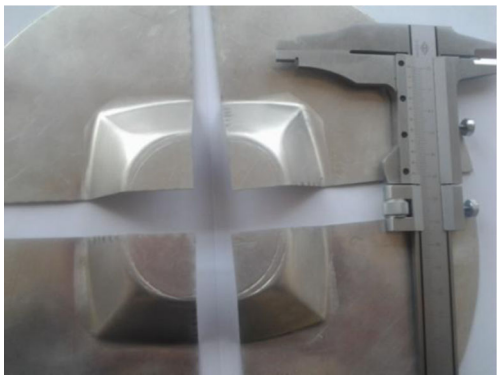

Fig. 12 Measurement method of the wall thickness

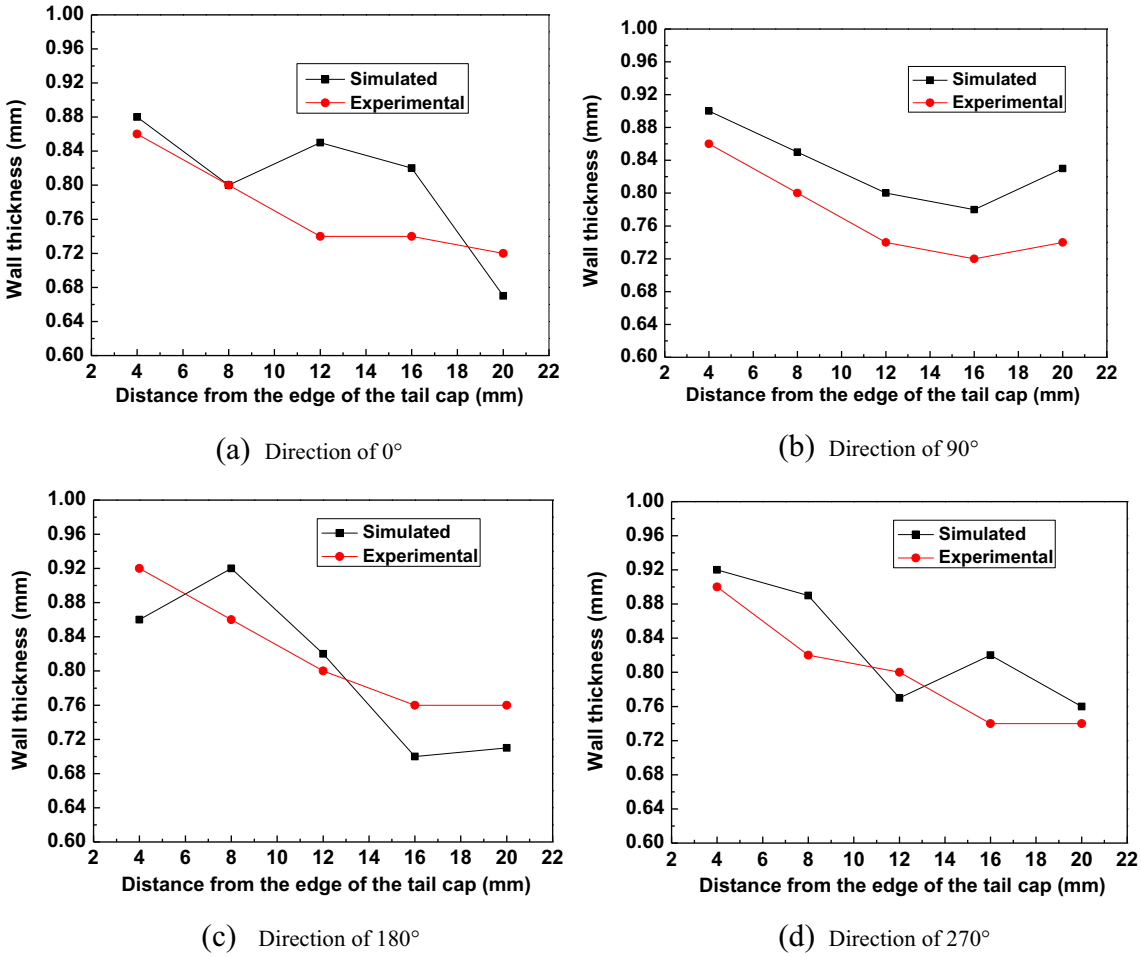

Fig. 13 Wall thickness distribution of the experiment and the simulation result. **a** Direction of 0 **b** Direction of 90° **c** Direction of 180° **d** Direction of 270°

of each point is measured by the caliper, see Fig 12). Figure 13 shows the measured value of the experiment and the simulation results. From Fig. 13, the wall thickness does not decrease very much from 1 mm and its distribution has the trend that the closer (to the tail cap) part is thicker than the farther part. As the roller goes further away from the tail cap along the axial direction, the radius distance it moves is longer (formula (5), so the roller affects more significantly on the farther part (from the edge of the tail cap) of the wall and makes it become thinner. The maximum deviation of the wall thickness between the simulated and the experimental results is no more than 15 %.

5 Conclusions

The square cross-section cone hollow spinning process is investigated by FEM and experiments. The conclusions are as follows:

1. The finite element model for square cross-section cone hollow spinning is established with the deduced roller path boundary condition and the accuracy of the finite element model is verified by the spinning experiment. Both the forming geometric dimensions and the distribution of the wall thickness between the simulation and the experiment agree well to each other with maximum deviation less than 5 and 15 %, respectively.
2. The stress and strain fields show that the residual stress on the surface of the workpiece is smaller after square cross-section cone hollow spinning and the maximum deformation locates on the axisymmetric center area of the slope surfaces, which is one of the reasons to make the side of the cross-section become a large radius arc.
3. The wall thickness of the square cross-section cone does not decrease very much from 1 mm, and its distribution has the trend that the closer (to the tail cap) part is thicker than the farther part.
4. The control of straightness of the cross-section edge and the surface quality for the square cross-section cone

formed by hollow spinning will be investigated in a follow-up report.

Acknowledgements This work was financially supported by the Open Foundation of Zhejiang Provincial Key Lab of Part Rolling Technology, China (No. ZKL-PR-200301), and the authors wish to express their gratitude.

References

1. Wong CC, Dean TA, Lin J (2003) A review of spinning, shear forming and flow forming processes. Int J Mach Tools Manuf 43(14):1419–1435
2. Kwiatkowski L, Tekkaya AE, Kleiner M (2013) Fundamentals for controlling thickness and surface quality during dieless necking-in of tubes by spinning. CIRP Ann-Manuf Technol 62(1):299–302
3. Molladavoudi HR, Djavanroodi F (2011) Experimental study of thickness reduction effects on mechanical properties and spinning accuracy of aluminum 7075-O, during flow forming. Int J Adv Manuf Technol 52(9–12):949–957
4. Huang CC, Hung JC, Hung C, Lin CR (2011) Finite element analysis on neck-spinning process of tube at elevated temperature. Int J Adv Manuf Technol 56(9–12):1039–1048
5. Akio S, Hirohiko A (2012) Control of wall thickness distribution by oblique shear spinning methods. J Mater Process Technol 212(4): 786–793
6. Fazeli AR, Ghoreishi M (2011) Statistical analysis of dimensional changes in thermomechanical tube-spinning process. Int J Adv Manuf Technol 52(5–8):597–607
7. Wang L, Long H (2013) Roller path design by tool compensation in multi-pass conventional spinning. Mater Des 46:645–653
8. Lin W, Hui L (2011) Investigation of material deformation in multi-pass conventional metal spinning. Mater Des 32(5):2891–2899
9. Lin B, Gu J, Zhou S, Liu J, Cai W, Fang L (2011) Research on process of multi-pass draw-spinning of hyper-hemispherical shell Jixie Gongcheng Xuebao. (Chin J Mech Eng) 47(6):86–91 (in Chinese)
10. Jiang SY, Zheng YF, Ren ZY, Li CF (2009) Multi-pass spinning of thin-walled tubular part with longitudinal inner ribs. Trans Nonferrous Metals Soc China 19(1):215–221
11. Jiang S, Ren Z, Li C, Xue K (2009) Role of ball size in backward ball spinning of thin-walled tubular part with longitudinal inner ribs. J Mater Process Technol 209(4):2167–2174
12. Xia QX, Cheng XQ, Hu Y, Ruan F (2006) Finite element simulation and experimental investigation on the forming forces of 3D non-axisymmetrical tubes spinning. Int J Mech Sci 48(7):726–735
13. Xia QX, Xie SW, Huo YL, Ruan F (2008) Numerical simulation and experimental research on the multi-pass neck-spinning of non-axisymmetric offset tube. J Mater Process Technol 206(1–3):500–508
14. Xia Q, Cheng X, Long H, Ruan F (2012) Finite element analysis and experimental investigation on deformation mechanism of non-axisymmetric tube spinning. Int J Adv Manuf Technol 59(1–4): 263–272
15. Xia QX, Lai ZY, Long H, Cheng XQ (2013) A study of the spinning force of hollow parts with triangular cross sections. Int J Adv Manuf Technol 68(9–12):2461–2470
16. Wu Xiaoyu, Numerical simulation and experimental research of the hollow part with four arc-typed cross-section by spinning, Master Thesis, South china University of Technology, 2010. (in Chinese)
17. Shimizu I (2010) Asymmetric forming of aluminum sheets by synchronous spinning. J Mater Process Technol 210(4):585–592
18. Yixuan TAN, Saiyi LI (2012) Finite element simulations of deformation behavior in equal channel angular pressing using a rotated die. Acta Metall Sin (English letters) 25(5):357–364